The latest version is at http://www.jbc.org/cgi/doi/10.1074/jbc.M117.781492

Nuclear insulin-like growth factor 1 receptor phosphorylates proliferating cell nuclear antigen and rescues stalled replication forks after DNA damage

Ahmed Waraky[1], Yingbo Lin[1], Dudi Warsito[1], Felix Haglund[1], Eiman Aleem[1, 2, 3, 4], and Olle Larsson[*1]

[1] Department of Oncology-Pathology, Cancer Center Karolinska, Karolinska institutet, Stockholm, Sweden.

[2] Institute of Molecular Medicine at Phoenix Children's Hospital,

[3] University of Arizona College of Medicine-Phoenix, Department of Child Health, Phoenix, Arizona, USA.

[4] Alexandria University, Faculty of Science, Department of Zoology, Alexandria, Egypt.

*Corresponding authors: Olle Larsson, olle.larsson@ki.se

Key words: IGF-1, PCNA, DNA damage, phosphorylation, post-translational modification, ubiquitination

Abstract

We have previously shown that the insulin-like growth factor 1 receptor (IGF-1R) translocates to the cell nucleus, where it binds to enhancer-like regions and increases gene transcription. Further studies have demonstrated that nuclear IGF-1R (nIGF-1R) physically and functionally interacts with some nuclear proteins, *i.e.* the lymphoid enhancer–binding factor 1 (Lef1), histone H3, and Brahma-related gene-1 proteins. In the present study, we identified the proliferating cell nuclear antigen (PCNA) as a nIGF-1R–binding partner. PCNA is a pivotal component of the replication fork machinery and a main regulator of the DNA damage tolerance (DDT) pathway. We found that IGF-1R interacts with and phosphorylates PCNA in human embryonic stem cells and other cell lines. *In vitro* MS analysis of PCNA co-incubated with the IGF-1R kinase indicated tyrosine residues 60, 133, and 250 in PCNA as IGF-1R targets, and PCNA phosphorylation was followed by mono- and polyubiquitination. Co-immunoprecipitation experiments suggested that these ubiquitination events may be mediated by DDT-dependent E2/E3 ligases (*e.g.* RAD18 and SHPRH/HLTF). Absence of IGF-1R or mutation of Tyr-60, Tyr-133, or Tyr-250 in PCNA abrogated its ubiquitination. Unlike in cells expressing IGF-1R, externally induced DNA damage in IGF-1R–negative cells caused G1 cell cycle arrest and S-phase fork stalling. Taken together, our results suggest a role of IGF-1R in DDT.

The insulin-like growth factor 1 receptor (IGF-1R) is a receptor tyrosine kinase. Upon ligand binding, membrane-bound receptors activate the phosphatidylinositol 3-kinase (PI3K)/Akt and mitogen-activated protein kinase (MAPK)/Erk signaling pathways (1).

We have previously shown that SUMOylation of IGF-1R (at Lys1025, Lys1100 and Lys1120) leads to increased transcriptional activity due to nIGF-1R binding to enhancer-like sequences (2). Mutations of the three *IGF1R* SUMO binding residues decreased nuclear transcriptional activity but did not affect the canonical signaling pathways (PI3K/Akt and MAPK/Erk) of the cell membrane IGF-1R. nIGF-1R has also been shown to associate to the LEF1 transcription factor and phosphorylate histone H3 (3,4). While canonical IGF-1R signaling is well characterized, the functional context of nIGF-1R is still poorly understood.

In this study we sought to identify potential nIGF-1R binding partners. For this purpose we immunoprecipitated IGF-1R from human embryonic stem cells (hESCs) and analyzed receptor associated proteins by mass spectrometry. One of the identified proteins was the proliferating cell nuclear antigen (PCNA), a nuclear protein that assembles in a homo-trimetric ring structure encircling the DNA double helix and functions as a mobile sliding clamp to recruit other proteins (such as DNA polymerases and ligases) during DNA replication (5). If unresolved, replication fork stalling caused by replication stress or DNA damage agents could induce genomic instability. PCNA is a principal component in the cellular response to replication fork stalling, and its functionality is tightly regulated in this respect (6-8).

Ubiquitination of PCNA has been shown to regulate various DNA damage tolerance (DDT) mechanisms. PCNA monoubiquitination induces switching to low-fidelity DNA polymerases which bypass DNA lesions (translesion synthesis, TLS). Polyubiquitination is believed to initiate the more complex template switching (TS) operation, wherein the intact sister strand is utilized to extend past the lesion (9-11).

Mono- and polyubiquitination of PCNA are mediated by two distinct sets of E2 (ubiquitin-conjugating enzyme) and E3 (ubiquitin-protein ligase) enzymes that operate in a linear fashion (12). PCNA is first monoubiquitinated by RAD6 (E2) and RAD18 (E3) (13-15), followed by K63 polyubiquitin-linkage by UBC13-MMS2 (a

E2 heterodimer) and HTLF or SHPRH (E3) (8,9,16-18)

In this study we demonstrate that IGF-1R directly phosphorylates three PCNA tyrosine ($Y^{60, 133, 250}$) residues. This phosphorylation leads to mono- and polyubiquitination. In addition, our results suggest that IGF-1R contribute to rescue of replication fork stalling in cells exposed to DNA damage.

Results

IGF-1R is expressed in cell nucleus of hESC

The nuclear localization of IGF-1R varies between cell types. Using immunoblotting of IGF-1Rβ in subcellular fractionations of human embryonic stem cell line H1 (WA01) hESCs (designated hESC henceforth). IGF-1R was found in both nuclear and membrane fractions of the cell line (Figure 1A). This was supported by immunofluorescence microscopy of IGF-1R, which showed clear fluorescence signals within the hESC nucleus (Figure 1B). This result was further supported by analysis of R+ and R- cells. These cell lines are *igf1r* knockout MEF cells, stably transfected with (R+) and not transfected with *IGF1R* (R-).

IGF-1R associates with PCNA in the cell nucleus

To investigate the role of nIGF-1R we sought to collect IGF-1R binding partners by immunoprecipitation (IP) of IGF-1R from hESC and identify them by liquid chromatography and mass spectrometry (LC-MS). IP of IgG served as a negative control. The immunoprecipitated proteins were eluted, separated by SDS-PAGE and stained with Coomassie Blue. Ten prominent gel bands observed in the IGF-1R sample but not the IgG sample were excised (Figure S1A). After LC-MS, multiple potential binding partners were identified including e.g. 14-3-3 proteins (previously described to bind IGF1-R (19)), heat-shock associated proteins, Elongation factor 2 (proposed target of IGF-1R signaling (20)), histone H4 and PCNA (Figure S1B). We decided to focus on PCNA because it exhibited several unique peptides and high coverage (Figure S1B).

The association of IGF-1R with PCNA was confirmed using IP with anti-IGF-1R and reciprocal IP with anti-PCNA, followed by immunoblotting for PCNA and IGF-1R, respectively (Figure 1C). Nuclear association was confirmed by Co-IP after subcellular fractionation (Figure S1C-D) and *In situ* PLA of IGF-1R and PCNA (Figure 1D). PLA showed clear signals abundantly located to the cell nuclei.

Next, we used R+ and R- cells to support the association between IGF-1R and PCNA (Figure 1E). While R+ exhibited this association, R- expectedly did not. The percentage of cells in S-phase and the expression level of PCNA (control blot) were similar in the two cell lines (Figure S2A-B). As the R+ cell line is a stable *IGF1R* transfectant produced from R- cells in the early '90s (21,22), we verified the observed IGF-1R-PCNA interaction in a newly transfected R- cell line (here denoted R-WT). R-EV represents empty vector control (Figure S2C).

Because R+ and R- cells provide an excellent cell system for comparison of the effect of presence and absence of IGF-1R, they were used as lead and control cell lines for investigation of IGF-1R-PCNA-dependent events. Selected findings were validated on other human and mouse non-engineered cell lines, including hESC.

IGF-1R directly phosphorylates PCNA on Y^{60}, Y^{133} and Y^{250}

IGF-1R is an established receptor tyrosine kinase in the cell membrane, but was recently shown to exert kinase activity also in the cell nucleus by directly phosphorylating histone H3Y41 (4). Consequently, we investigated whether nIGF-1R might phosphorylate PCNA. First we compared PCNA tyrosine phosphorylation status in R+ with R- cells. IP of PCNA followed by detection of phosphotyrosine showed that PCNA is phosphorylated only in R+, not in R- cells (Figure 2A, top panel), as shown by several bands in R+ cells between 30-60 kDa. Reciprocal Co-IP confirmed this finding (Figure 2A, bottom panel). These results indicate that the expression of IGF-1R is necessary for tyrosine phosphorylation of PCNA, but do not determine whether this is mediated through the canonical IGF-1R signaling or directly by the nuclear receptor.

To investigate whether IGF-1R phosphorylates PCNA directly, an *in-vitro* kinase assay was used. As shown, recombinant IGF-1R kinase domain was able to tyrosine phosphorylate recombinant PCNA (Figure 2B). The presence or absence of ATP in the reactions was used as control. The specificity of IGF-1R phosphorylation was further confirmed by adding IGF-1R inhibitor (NVP-AEW541) to the reaction (Figure S3A). As a positive control for the IGF-1R kinase activity in-vitro we showed that it phosphorylated itself (a bona fide substrate) under such conditions (Figure 3B).

In order to identify the specific PCNA tyrosine residue(s) being phosphorylated by nIGF-1R, we utilized MS analysis of

recombinant PCNA after in-vitro phosphorylation by recombinant IGF-1R. Recombinant PCNA without IGF-1R was used as negative control. The result reveals that residues Y^{60}, Y^{133} and Y^{250} were phosphorylated by the IGF-1R kinase (Figure 2C). These data indicate that IGF-1R is capable of directly phosphorylating PCNA, suggesting that PCNA is a substrate of the nuclear IGF-1R tyrosine kinase activity. To confirm these results, the potential function of the Y^{60}, Y^{133} and Y^{250} residues will be considered below.

IGF-1R activity does not affect PCNA stability

Nuclear epidermal growth factor receptor (EGFR) has previously been reported to control PCNA stability through Y^{211} phosphorylation (23). To investigate whether IGF-1R mediated PCNA phosphorylation affected PCNA stability, R+ cells were treated with either IGF-1 or NVP-AEW541 for 3 and 24 hours. However, neither IGF-1R stimulation nor inhibition altered the PCNA levels (Figure 2D). Additionally, R+ and R- cells showed similar PCNA levels. These data suggest that IGF-1R does not affect PCNA stability.

Nuclear IGF-1R mediated phosphorylation marks PCNA for ubiquitination

Posttranslational modification of PCNA by mono- and polyubiquitination has been shown to control various PCNA functions, including the DDT pathway (see introduction). Using co-IP experiments we observed mono- and polyubiquitinated PCNA in R+ but not in R- cells. (Figure 3A).

To investigate possible involvement of IGF-1R kinase activity in ubiquitination of PCNA. R+ cells were treated with either NVP-AEW541 or IGF-1 for 3h, followed by immunoprecipitation of PCNA and detection of phosphotyrosine and ubiquitin. IGF-1 treatment clearly increased both PCNA phosphorylation and ubiquitination, while inhibition of IGF-1R reversed/decreased these effects (Figure 3B).

In order to confirm the nuclear function of IGF-1R in inducing PCNA phosphorylation and subsequent ubiquitination, PCNA from cytoplasmic and nuclear fraction of R+ cells was pulled down using IP. As shown in Figure S5A-B, PCNA only from the nuclear fraction was tyrosine phosphorylated and ubiquitinated. Further confirmation was achieved by using R-TSM cells; (R- transfected with triple-SUMO-site-mutated IGF1R cell line). Just recently we showed that R-TSM cells exhibited diminished

nuclear gene regulatory effects of IGF-1R while retaining IGF-1R kinase-dependent signaling (2,24).

IGF-1R from R+ and R-TSM was pulled down using IP and equal amounts of it was subjected to in-vitro kinase assay using recombinant PCNA as substrate (Figure S4C). As shown, only IGF-1R from R-WT was able to phosphorylate PCNA (Figure S4C). Incubation with TSM IGF-1R did not lead to any detectable phospho-PCNA signal. IP from R- was used as negative control. We then analyzed ubiquitination of PCNA in these cell lines. Only PCNA from R+ cells was phosphorylated and ubiquitinated (Figure S4D). Taken together, the results suggest that nIGF-1R-induced phosphorylation of PCNA is involved in its ubiquitination. The inability of TSM IGF-1R to phosphorylate PCNA is in line with observed decrease in phosphorylation of histone H3 in Hela cells transfected with TSM IGF-1R (4).

Inhibition of the MAPK/Erk and the PI3K/Akt pathways using the inhibitors U0126 and LY2942002, respectively, did not decrease PCNA ubiquitination as compared to the untreated control (Figure S5A-B), which supports the notion that PCNA ubiquitination is mediated by nuclear IGF-1R and not by the canonical signaling of membrane IGF-1R.

PCNA Y^{60}, Y^{133} and Y^{250} are essential for recruitment of DDT-dependent ligases and ubiquitination

Mono- and polyubiquitination of PCNA byRAD6 (E2)-RAD18 (E3) and UBC13 (E2)-SHPRH/HLTF (E3), respectively, have been shown to regulate PCNA function through the DDT pathway (9,10). Using Co-IP experiments, we showed the association of UBC13 (E2) and SHPRH/HLTF (E3) with PCNA in R+ but not R- cells (Figure 3C). This suggests that nIGF-1R-dependent PCNA polyubiquitination may be mediated by these ligases. Similar results were also obtained for the monoubiquitinRAD18 (E3) ligase and the main TLS polymerase DNA polymerase η (Figure 3C). As a control, the expression of ligases in whole cell lysates was investigated by immunoblotting. Essentially similar levels are detected in R+ and R- cells (Figure S6A). A separate experiment on association of SHPRH, HTLF and RAD18 with PCNA, and ligase expression in whole cell lysates, is presented in Figure S7A. This experiment also involved a random nuclear protein (i.e. p27), which did not Co-IP with PCNA (Figure S7A). IGF-1 stimulation increased the binding of SHPRH/HLTF, RAD18 and DNA Poly η to PCNA, whereas inhibition with NVP-AWE541 decreased it (Figure S7B).

The importance of PCNA Y^{60}, Y^{113} and Y^{250} phosphorylation sites for IGF-1R-PCNA interaction and subsequent modifications was then investigated by site-specific mutations. R+ cells were transfected with eGFP-PCNA constructs representing either wild type *PCNA* or mutated *PCNA,* resulting in a tyrosine replaced by a phenylalanine (Y60F, Y133F, Y250F or triple mutated Y60F-Y133F-Y250F, denoted Y-Tpl). Exogenous PCNA was pulled down using Co-IP with anti-GFP. In contrast to the exogenous wild type PCNA, all 4 mutants abolished IGF-1R/interaction, PCNA-phosphorylation and ubiquitination, as well as binding of SHPRH/HLTF and RAD18 ligases (Figure 3D). This suggests that phosphorylation of all three tyrosine residues is necessary for nIGF-1R/PCNA interaction. Control blots of ligase expression in lysates of the transfected cells are shown in Figure S6B.

Together with our findings that IGF-1R associates with PCNA in cell nuclei (Figure 1), and has the capacity to directly phosphorylate PCNA (Figure 2; Figure S3), it appears that the nuclear-localized receptor serves as the kinase and thereby triggers the subsequent ubiquitination.

To verify the functional role of mutated PCNA constructs in DNA replication, we investigated GFP-gated Y-Tpl in R+ cells by FACS analysis after BrdU/DAPI labeling. Upon synchronization by serum starvation, the cells were released and analyzed at different time points (0-20 h). As shown in Figure S8, the cells progressed from G1 to and through the S phase. After 20 h, many cells reentered the G1 phase. Similar results were seen for the other (single mutated) eGFP-PCNA transfected cell lines (data not shown).

IGF-1R regulates PCNA ubiquitination after DNA damage

Since PCNA ubiquitination has been coupled to the DDT pathway mainly after DNA damage that induce replication fork stalling, we next sought to explore the potential role of nIGF-1R mediated PCNA ubiquitination in response to UV treatment. R+ and R- cells were exposed to UV irradiation, 30 mJ/cm^2, for 30 seconds, followed by 1h exposure-free incubation. PCNA in R- cells did not exhibit any ubiquitination in response to UV irradiation (Figure 4A). Conversely, the base-line ubiquitination of PCNA in R+ cells was increased substantially by UV, but was attenuated if NVP-AWE541 was added prior to the irradiation (Figure 4A). Similarly, R+ cells showed a strong induction of PCNA ubiquitination after treatment with the alkylating agent methyl methanesulfonate (MMS) (Figure S9). This effect was abolished by IGF-1R inhibition. Thus, DNA damage-induced ubiquitination of PCNA was dependent on IGF-1R activity.

IGF-1R is involved in DDT pathway

Our next step was to investigate role of IGF-1R in DDT pathway. One method for assessing the efficiency of the DDT pathways is to measure the speed of replication restart after induction of DNA damage. This measures the cell's ability to tolerate DNA damage upon encountering polymerase blocking lesions. To assess the functional role of IGF-1R in the DDT pathway, we applied the DNA fiber-labeling method to measure replication fork progression after MMS-induced DNA damage in R+ and R- cells. Briefly, cells were incubated with two different halogenated nucleotides, chlorodeoxyuridine (CldU) and iododeoxyuridine (IdU), which are incorporated into nascent DNA at replication forks before and after inducing DNA damage by MMS as schematically shown in Figure 4B. The speed of DNA replication restart was estimated as the IdU/CIdU ratios of the lengths of labeled nascent replication tracts before (CIdU) and after (IdU) induction of DNA damage. MMS treatment delayed DNA replication by 60% in R+ cells, but by as much as 90% in R- cells (Figure 4C). Thus, R+ cells have a more efficient DDT pathway than R- cells.

To further characterize the role of IGF-1R in the DDT pathway we used FACS analysis, after BrdU/PI labeling, to determine the effect of DNA damage upon cell cycle progression. R+ and R- cells, were synchronized by serum depletion, and then treated with MMS or DMSO (control) for 6h. Upon serum repletion, the R+ and R- control cells progressed through the cell cycle (Figure 5A and B). Treatment with MMS slowed down the cell cycle progression only in R+ cells (Figure 5 A-B). No increase in percentage of cells in G1 was seen in R+ cells. In R- cells, MMS treatment substantially inhibited cell cycle progression by inducing G1-cell cycle arrest, decreasing the number of cells in S-phase, and almost blocking the progression of cells into the G2-phase (Figure 5A and B). Further support for this response was obtained using unsynchronized cells. R+ and R- cells were pulse-labeled with BrdU for 1h, followed by treatment with DMSO or MMS for 6h (Figure 5C). The BrdU labeled cells were then gated (green dots), and the progression of the gated cells through S-phase after treatment was investigated. In a pattern that was basically similar to that in synchronized cells, the R+ cells were able to progress from G1/S phase to S/G2 phase at a slower rate after MMS treatment, while R- cells collapsed in G1/S phase, with minimal cells progression towards S/G2 phase.

To further investigate the role of IGF-1R in DDT, we analyzed the connection between IGF-1R activity and PCNA phosphorylation

in cells entering S-phase. We used the same experimental condition as described in Figure 5A-B. Serum-starved R+ and R- cells were restimulated in 12h for maximal S-phase synchronization (Figure S10A). We first investigated S-phase cells under spontaneous fork stalling (i.e. without DNA damage exposures). After IP of PCNA, IGF-1R, p-Tyr and PCNA were detected (Figure S10B). In serum starved R+ cells (indicated as G1) there was a slight IGF-1R/PCNA interaction and no PCNA phosphorylation. In contrast, R+ cells in S-phase (indicated as S) showed a much stronger association between IGF-1R and PCNA as well as a clear PCNA phosphorylation. However, upon addition of NVP-AEW541, p-Tyr PCNA was almost deleted (Figure S10B). No PCNA phosphorylation was seen in R- cells. Next, we investigated S-phase cells under condition of fork stalling collapse, as induced by a 6h MMS treatment (cf. Figure 5A and B). As shown in Figure S10C, MMS treatment drastically increased phosphorylation of PCNA as compared to the negative controls. Simultaneous treatment with the IGF-1R inhibitor abrogated the MMS-induced response. No effects were observed in R- cells (Figure S10C). These data support a role IGF-1R in DDT through phosphorylation of PCNA.

IGF-1R/PCNA interaction and PCNA ubiquitination in cells with endogenous IGF-1R

The cell lines SNL (a MEF cell line) and a Gm02808 (human fibroblasts) were compared with hESC and R+/R- cells. Similar to hESC and R+, the IGF-1R-PCNA complex was detected in SNL and GM02808 (Figure 6A). They all exhibited PCNA phosphorylation and ubiquitination in a pattern similar to R+, but at varying levels (Figure 6B). And similar results were also shown regarding PCNA association with DDT-dependent E2/E3 ligases (Figure 6C). The expression levels of the various E2/E3 ligases in whole cell lysates of SNL, GM02808 and hESC cells are shown in Figure 6D.

Discussion

The role of nuclear-localized IGF-1R in normal physiology and disease is still poorly understood. Here we identified and characterized a novel potential role of nIGF-1R. We found that IGF-1R interacts with and phosphorylates PCNA on three tyrosine residues (Y^{60}, Y^{133} and Y^{250}), which was followed by ubiquitination. We also provided evidence that IGF-1R increases tolerance to DNA damage (DDT). The interaction between IGF-1R and PCNA may play a role in this respect, as we could show IGF-1R-dependent increase in

phosphorylation of PCNA in cells entering S-phase under conditions of spontaneous fork stalling and fork stalling collapse as well. Together our findings suggest a mechanistic link between IGF-1R/PCNA interaction and DDT.

Our opinion that IGF-1R-dependent phosphorylation of PCNA is mediated by nIGF-1R and not through the canonical signaling pathways via the cell membrane receptor is supported by the followings findings; (1) IGF-1R and PCNA co-localize exclusively in cell nuclei; (2) IGF-1R phosphorylates PCNA in vitro in the absence of other kinases; (3) PCNA is phosphorylated in cells expressing WT-IGF-1R but not in those expressing TSM-IGF-1R; and (4) inhibition of PI3K/Akt and MAPK/Erk activity by specific inhibitors did not abrogate phosphorylation and ubiquitination of PCNA.

Other receptor tyrosine kinases have been shown to translocate to the nucleus and phosphorylate PCNA on different sites (25). Nuclear EGFR was reported to phosphorylate PCNA on Y^{211}, regulating PCNA stability and inhibiting DNA mismatch repair (26). The tyrosine kinase c-ABL has also been shown to phosphorylate PCNA on Y^{211}, increasing DNA synthesis activity (27). These results are in line with the notion that PCNA phosphorylation may regulate different functions of PCNA in DNA-repair and replication, and the discrepancies may be explained by the different tyrosine residues modified.

The identified tyrosine phosphorylated sites (Y^{60}, Y^{133} and Y^{250}) have been described in a number of previous studies mediating other functions. A study of global tyrosine phosphorylation identified a significant PCNA Y^{250} phosphorylation after EGF stimulation in HeLa-cells (28). PCNA Y^{133} was shown to be important for PCNA interaction with MCM10, a key component of the pre-replication complex (29) . It was shown that PCNA is phosphorylated prior to binding to DNA replication sites (30), suggesting a possible role in replication fork formation. Both Y^{133} and Y^{250} have previously been shown to participate in p21 interaction (31). Interestingly, our site-directed mutagenesis revealed that Y^{60}, Y^{133} and Y^{250} were all crucial for IGF-1R/PCNA interaction and subsequent ubiquitination of PCNA. This points to a critical role for all three sites, as suggested by the location of Y^{250} and Y^{133} tyrosine sites, which appear to lie within the hydrophobic groove on the front side adjacent to the interdomain-connecting loop (IDCL) where most of PCNA interacting proteins bind to (32) (Figure 7A).

Ubiquitination of PCNA has repeatedly been shown to regulate DDT. In response to replication fork stalling, PCNA polyubiquitination is thought to trigger the DDT pathway to avoid replication fork collapse (9,11). Replication fork stalling could result from a variety of reasons including; DNA damage, or defects in the replication machinery (33). In addition, recent studies have showed that nucleotide deprivation can induce replication fork stalling (33,34). Thus increased proliferation caused by the high expression of IGF-1R may induce replication fork stalling through nucleotide deprivation. This might explain the presence of PCNA ubiquitination and association with E2/E3 ligases of the DDT pathway under basal growth conditions. The cell lines investigated by us (hESC, MEFs and human fibroblast cell lines) do all show a substantial expression IGF-1R, even in absence of induced exogenous DNA damage. This is in line with findings of detected PCNA ubiquitination in Xenopus extracts during unperturbed DNA replication (35), and in human cell lines not exposed to exogenous DNA damage (36). Thus, even in the absence of exogenous DNA damaging agents forks stalling occurs in a significant fraction of the cell division cycles (33).

Our finding that IGF-1R was required for PCNA ubiquitination in response to DNA damage by UV treatment is supported by previous studies showing that IGF-1R activation is associated with increased radioresistance both *in- vitro* and *in-vivo* (37,38). However, it cannot be excluded that other protein kinases can phosphorylate and regulate DDT through ubiquitination of PCNA in other cell systems. In yeasts, which lack IGF-1R, PCNA ubiquitination by DDT E2/E3 ligases has been demonstrated (9-11).

The importance of PCNA in maintaining genomic stability has been demonstrated in a number of studies. An affected family carried a homozygous *PCNA* missense mutation, resulting in PCNA S228I (39) showed a decreased ability to sustain UV radiation through a decreased PCNA affinity for DNA metabolic enzymes, with no effects on DNA replication. Clinically, this was reflected by genomic hypermutability. This suggests that PCNA residue S228 is important for DNA repair rather than proliferation. This is compatible with our finding that the Y^{60}, Y^{133} and Y^{250} mutants affect PCNA ubiquitination only, not DNA replication/proliferation.

Deficiencies in genes regulating the DDT pathway have been shown to be important for maintaining genomic stability. HLTF-deficient mouse embryonic fibroblasts showed elevated chromosome breaks and fusions after MMS treatment (8). Also,

reduction of either SHPRH or HLTF expression enhanced spontaneous mutagenesis in human fibroblasts. Furthermore, mutation of the XPV gene, encoding DNA Pol η in humans, results in a variant type of *Xeroderma pigmentosum (40)*. Patients with this disease variant are hypersensitive to UV damage, with reduced ability to elongate nascent DNA strands upon UV-irradiation, and are predisposed to cancer (9,41-43).

Genetic syndromes with deficiencies in genes regulating genomic stability are being increasingly recognized for their relevance in the aging process. The connection between IGF-1R signaling and longevity was made in genetically modified mice (44) and there is an ongoing discussion about the potential link between somatotropic axis signaling (GH/IGF), DNA repair and DDT (45,46). While multiple factors may influence ageing in genetically altered models, IGF-1R might be of some importance for normal ageing through affecting DDT. A closer investigation on this matter is warranted.

In response to replication stress or external DNA damage, IGF-1R-mediates PCNA ubiquitination, as proposed in the model shown in Figure 7B. nIGF-1R phosphorylates PCNA on three tyrosine residues ($Y^{60,133,250}$), which in turn targets PCNA for mono- and poly ubiquitination, possibly by the DDT E2/E3 ligases. The phosphorylation of all three tyrosine residues (Y60, 133, 250) appears to be critical for subsequent nIGF-1R-PCNA interaction. IGF-1R aids in protecting the cells from replication fork stalling and therewith it may contribute to maintained genetic stability. The effect on DDT might be influenced by IGF-1R/PCNA interaction and associated PCNA modifications. Further studies are needed to explore this interaction closer.

Experimental procedures

Reagents

NVP-AEW541 (IGF-1R tyrosine kinase inhibitor) was purchased from Cayman Chemical (Ann Arbor, MI, USA). Insulin-like growth factor-1 (IGF-1), U0126 (MEK1/2 inhibitor), dimethylsulphoxide (DMSO), LY2942002 (PI3K inhibitor), polybrene, mitomycin C and β-mercaptoethanol were all purchased from Sigma-Aldrich (St. Louis, MO, USA). Basic fibroblast growth factor (bFGF) was bought from R&D systems (Minneapolis, MN, USA) and methyl methanesulfonate (MMS) from Santa Cruz Biotechnology (Santa Cruz, CA, USA). NVP-AEW541, U0126, LY2942002 and MG132 were dissolved in DMSO and used at a concentration of 1μM,

5μM, 20μM and 5μM, respectively. IGF-1 and bFGF were dissolved in 0.1% bovine serum albumin (BSA) in PBS (Hyclone, Logan, UT) and used at a final concentration of 100 ng/ml and 4ng/ml, respectively. RPMI-1640, F-12, Dulbecco's modified Eagle's medium (DMEM), collagenase and cell culture supplements, including fetal bovine serum (FBS), non-essential amino acids (NEAA), knockout serum replacement (KSR), L-glutamine, puromycin and blasticidin were purchased from Invitrogen (Paisley, UK). mTeSR™1 stem cell medium was from Stem Cell Technologies (Grenoble, France).

Cell cultures

Mitotically inactive feeder cells were established by treating mouse embryonic fibroblast feeder cells (SNL, kindly provided by Dr. K. Wiman, Karolinska Institutet, Stockholm, Sweden) with 10μg/ml mitomycin C and cultured in DMEM with 10% FBS and 1% NEAA. H1 (WA01) hESC (WiCell Research Institute Inc., Madison, WI, USA) cells were maintained as described in (47). Briefly cells were seeded on inactivated SNL feeder cells in DMEM-F12 with 20% KSR in 1 mM L-glutamine, 10 mM NEAA, 50 mM β-mercaptoethanol, and 4 ng/ml bFGF. All hESCs experiments were conducted between passage numbers 27 and 60. For feeder-free conditions, cells were passaged every 4-6 days using collagenase and plated on Geltrex™ matrix in mTeSR™1 Medium in feeder-free conditions as described in (47).

The platinum-A retroviral packaging cell line was purchased from Cell Biolabs Inc. (San Diego, CA, USA). Mouse embryonic fibroblasts (MEF) *igf1r* - /- (R-) and R- cells overexpressing IGF1R (R+) were from Dr. R. Baserga (Thomas Jefferson University, PA, USA). The R-WT (R- with newly transfected WT IGF1R), R-TSM (R- transfected with SUMO-mutated IGF1R) and R-Puro (empty vector control) were obtained as described elsewhere (24). All cell lines were cultured in DMEM with 10% FBS, with the exception of Gm02808 being cultured in DMEM/F12 with 20% FBS. Platinum-A cells were additionally supplied with 1 μg/mL puromycin and 10 μg/mL blasticidin.

All cell lines were maintained at 37°C in a humidified atmosphere containing 5% CO_2 and checked for mycoplasma using MycoalertTM kit (Lonza, Basel, Switzerland). All human cell lines were short tandem repeat (STR) authenticated using AmpFLSTR® Identifiler® Plus kit (Applied Biosystems, Foster City, CA, USA), except for Gm02808 due to lack of STR reference.

Recombinant DNA techniques

PCNA cDNA sequence was PCR amplified from pEGFP-PCNA-IRES-puro2b (Addgene plasmids ID:26461) and inserted into linearized pBabe-puro empty vector (Cell biolabs, San Diego, CA) in between BamH I and EcoR I restriction sites using In-Fusion® Dry-Down PCR cloning kit (Clontech, Palo Alto, CA). The constructed pBabe-PCNA plasmid was expanded in E.coli and extracted using PureLink® HiPure Plasmid Filter Maxiprep kit (Invitrogen). Site-specific mutated PCNA expression plasmids were generated using the Quick-Change® Site-Directed Mutagenesis kit (Agilent Technologies, Santa Clara, CA) using the primers listed in Table S1. The successful introductions of specific point mutations were confirmed by sequencing at GATC Biotech (Konstanz, Germany). Expression plasmids with multiple point mutations were created through several rounds of single point mutagenesis.

Stable transfections

Platinum-A virus packaging cells were plated in antibiotic-free medium one day before and a medium change was performed 6 h before transfection. 30 µg plasmid DNA was mixed with 500 µl of 250 mM $CaCl_2$, and added to 500 µl of 2X BES-buffered saline (BBS) (Sigma-Aldrich). After incubation at room temperature (RT) for 30 min, the mixture with generated DNA precipitate was added dropwise to the cells, which were incubated in a CO_2 incubator at 37°C for 16 h, followed by medium change and additional 24h incubation.

R+ cells were seeded at low density in 6-well plates. Medium from the transfected Platinum-A cells containing the packaged retrovirus was collected, supplemented with 8 µg/ml polybrene, filtered through 0.45µm polysulfonic filters (Pall Corporation, Ann Arbor, MI) and added to the R+ cells for infection. A total of three infections were carried out with 24h incubation intervals. Transfected R+ cells were obtained by antibiotic selection using 2 µg/ml puromycin. The stable clones were generated at limited dilution in 96-well plates.

Immunoblotting

Cells were lysed in modified RIPA buffer (50 mM Tris pH 7.4, 150 mM NaCl, 1% NP-40, 1 mM EDTA, 0.25% sodium deoxycholate) containing protease (Roche, Mannheim, Germany) and phosphatase (Sigma-Aldrich) inhibitors, and processed as described in (48). Primary antibodies used in this research included rabbit anti-IGF-1R (#3024), rabbit anti- IGF-1Rβ (#3027) and mouse anti-PCNA (#2586) from Cell Signaling Technology; mouse anti-

phosphotyrosine (sc-7020), mouse anti-Ubiquitin (sc-8017), and goat anti-GFP (sc-5385) from Santa Cruz Biotechnology; mouse anti-UBC13 (#37-1100 from Zymed Laboratories South San Francisco, CA, USA); rabbit anti-PCNA (ab18197), rabbit anti-SHPRH (ab80129), rabbit anti-HLTF (ab155031), and rabbit anti-Pol eta (#ab154330) from Abcam, Cambridge, UK; and mouse anti-Rad18 (# WH0056852M1) from Sigma-Aldrich. Membranes were incubated with secondary anti-rabbit/mouse/goat IgG horseradish peroxidase-conjugated antibodies (NA934 and NA931 from GE Life Science and 31402 from Pierce Biotechnology) followed by signal detection using enhanced luminescence Hyperfilm-ECL (GE Life Science).

Cell fractionation

Subcellular fractionation for immunoprecipitation was prepared as described in (49) with some modifications. Briefly cytoplasmic fraction was achieved by lyzing cells in (10 mM HEPES pH 7.4, 10 mM KCl, 0.05% NP-40) buffer. The nuclear fraction was achieved by washing the pellet with same buffer, then lyzing in modified RIPA buffer.

Fractionation of membranous, cytoplasmic and nuclear components for western blotting was done using the Qiagen Qproteome Cell Compartment kit (Qiagen, Hilden, Germany). Subcellular fractionations were confirmed by immunoblotting for membranous Calnexin (rabbit anti-Calnexin, #2433 from Cell signaling Technology), cytoplasmic GAPDH or Hsp-90 (rabbit anti-GAPDH, sc-25778 from Santa Cruz); mouse anti-Hsp90 (ab13492 from Abcam, Cambridge, UK) or nucleic Histone H2A (rabbit anti- H2A, #2578 from Cell signaling Technology) as described above.

Immunoprecipitation

The following antibodies were crosslinked to magnetic Protein G Dynabeads using Dynabeads® antibody coupling kit #14311D (Invitrogen): mouse anti-IGF-1R (#556000), mouse anti-IgG (#555746, both from BD Biosciences, San Jose, CA); rabbit anti-PCNA (ab18197 from Abcam) and rabbit anti-IgG (sc-66931, Santa Cruz Biotechnology). Non-crosslinked antibodies included: rabbit anti-IGF-1Rβ (#3027), mouse anti-PCNA (#2586, both from Cell signaling Technology); mouse anti-IgG (554126 from Becton Dickinson); rabbit anti-IgG (sc-6693), goat anti-GFP (sc-5385) and mouse anti-P-Tyr (sc-7020, all from Santa Cruz Biotechnology).

After blocking with 0.1% BSA in PBS (Hyclone), 2-4 mg cell lysates were incubated with cross-linked antibody at

concentrations of 4-7 µg antibody/mg beads for 1h at 4°C. For non-crosslinked antibodies, lysates were incubated overnight at 4°C. The immune complexes were washed three times with lysis buffer and eluted by boiling in SDS sample buffer (Invitrogen). Subsequent immunoblottings were performed as described above.

In-vitro kinase assay

1 µg of N-terminal His-tagged recombinant IGF-1R kinase domain fusion protein (Millipore, Bedford, MA), or endogenous IGF-1R pulled down using IP, was incubated with 2 µg of N-terminal His-tagged PCNA fusion protein (Invitrogen) at 30 °C for 30 min in 30 µl of kinase buffer (60 mM HEPES at pH 7.9, 5 mM $MgCl_2$, 5 mM $MnCl_2$, 30 µM Na_3VO_4 and 1.25 mM DTT) in the presence of 20 µM ATP (all from Sigma-Aldrich). Omission of either His-tagged PCNA fusion protein, the IGF-1R kinase domain or ATP served as negative controls. The reactions were terminated by boiling in SDS sample buffer (Invitrogen), followed by separations in 10% SDS–PAGE and immunoblottings.

For analysis of PCNA posttranslational modifications, in-vitro kinase assays of His-tagged recombinant PCNA were carried out with or without the recombinant IGF-1R kinase domain. After SDS-PAGE separation and Coomassie blue staining, the bands corresponding to PCNA were cut out and compared by liquid chromatography-tandem mass spectrometry (LC-MS/MS) analyses as described below.

Immunofluorescence

hESCs were seeded on coverslips pre-coated with Geltrex, fixed in 4% buffered paraformaldehyde, permeabilized using 0.1% TritonX-100 and incubated overnight at RT with rabbit anti-IGF-1Rβ (#3027 from Cell signaling Technology) or mouse anti-IGF-1Rβ (#05-656 from Millipore). Cells were washed with PBS and incubated with goat anti-rabbit Alexa Fluor 594-conjugated antibody (#A11012) or goat anti-mouse Alexa Fluor 488-conjugated antibody (#A11029, both from Invitrogen) for 1h at RT. The coverslips were mounted using Vectashield mounting medium containing DAPI (Vector Laboratories, Burlingame, CA) for counterstaining purposes, and examined using an Axioplan 2 fluorescence microscope (Zeiss, Jena, Germany).

In situ proximity ligation assay (PLA)

hESCs were cultured and fixed on coverslips as described above. Permeabilization was done with 0.2% TritonX-100 for 30 min at RT, followed by incubation with blocking buffer for 30 min (5% BSA, 5% Donkey serum, 0.3% Triton in phosphate-buffered saline) and mouse anti-IGF-1Rβ (#05-656 from Millipore) or rabbit anti-PCNA

(#ab18197 from Abcam) at 4°C overnight. Duolink in situ PLA was conducted as previously described (Söderberg et al., 2006), using PLA probe anti-mouse minus and PLA probe anti-rabbit plus (OLINK Bioscience, Uppsala, Sweden).

Mass spectrometry

For hESCs cells, total cell lysates were used for immunoprecipitation of IGF-1R or IgG (negative control). Precipitates were separated with SDS-PAGE, and co-precipitated protein bands were visualized using Coomassie Blue. Ten prominent gel bands were exclusively seen in the IGF-1R lane (Figure S1A) and excised for further processing. Gel pieces were cut into small pieces and shrunk in acetonitrile. The samples were reduced at 56°C using 100 mM ammonium bicarbonate containing 10 mM DTT for 30 min. The supernatants were collected. Next, the samples were incubated in 100 mM ammonium bicarbonate containing 55 mM iodoacetamide at RT for 20 min in the dark. Then the gel pieces were shrunk once more and the supernatant was collected. Gel pieces were destained in a 1:1 mixture of 100 mM ammonium bicarbonate and acetonitrile for 30 min, followed by shrinking and aspiration of the supernatant. The gel pieces were then incubated on ice for 2h with 13 ng/µl trypsin (sequencing grade modified, Pierce Biotechnology) in 10 mM ammonium bicarbonate and 10% acetonitrile. Digestion was carried out at 37°C overnight. Peptides were extracted using 2 volumes of 1.67% formic acid in 67% acetonitrile at 37°C for 15 min. The extracts were dried in a SpeedVac and resuspended in 3% acetonitrile, 0.1% formic acid.

LC-MS was performed using a hybrid LTQ-Orbitrap Velos mass spectrometer (Thermo Scientific). For each LC-MS/MS run, the auto sampler (HPLC 1200 system, Agilent Technologies) dispensed 8 µl of solvent A, mixed for 10 min, and proceeded to inject 3 µl. Samples were trapped on a C18 guard desalting column (Agilent Technologies) and separated on a 15-cm long C18 picoFrit column (100 µm internal diameter, 5 µm bead size, Nikkyo Technos, Tokyo, Japan) installed on the nano-electrospray ionization source. Solvent A was 97% water, 3% acetonitrile and 0.1% formic acid; solvent B was 5% water, 95% acetonitrile and 0.1% formic acid. At a constant flow of 0.4 µl/min, the curved gradient went from 2% B up to 40% B in 45 min, followed by a steep increase to 100% B in 5 min.

The survey scan, performed in the Orbitrap with 30,000 resolution (and mass range 300-2000 m/z), was followed by data-dependent MS/MS (centroid mode) in two stages: first, the top five ions from the master scan were selected for collision-induced dissociation

(CID), using 35% normalized collision energy with ion trap mass spectrometry (ITMS) detection; then the same five ions underwent higher energy collision dissociation (HCD), using 37.5% normalized collision energy for iTRAQ or TMT labeled samples, 32.5% for label-free samples (7,500 resolution) with detection in the Orbitrap (FTMS). In addition, an ETD procedure was used where precursors underwent ETD fragmentation (instead of CID or HCD) provided they possessed sufficient charge density. Accordingly, only triply charged precursor ions with m/z < 650, quadruple charged ions with m/z < 900, quintuple charged ions with m/z < 950, or precursors with higher charge states were selected for ETD. Precursors were isolated with a 2 m/z window. Automatic gain control (AGC) targets were 1 x 106 ions for MS and for MS/MS 3 x 104 (CID) and 5 x 104 (HCD). The software Proteome Discoverer v.1.4, including Sequest, was used to search the human Uniprot database for protein identification, limited to a false discovery rate of 1%.

Cell synchronization and cell cycle analysis

Cells were plated at low density and allowed to grow for 24h. Then they were washed twice with PBS and incubated in serum-free medium for 24h to achieve G0/G1 synchronization, followed by release for 12h in medium containing 10% serum to synchronize cells at G1/S-Sphase. Cells were then treated for 6h with 1.2 mM MMS or vehicle.

The proportion of synchronized cells in S phase was measured by bromodeoxyuridine (BrdU, Sigma-Aldrich) incorporation, and G1 and G2 phases were measured by staining with propidium iodide (PI, Sigma-Aldrich) as previously described (50). Briefly, cells were pulse labeled with 100 µM BrdU for 1h before harvest. For flow cytometry, cells were washed with PBS, fixed with 70% ethanol overnight and stained with anti-BrdU (Becton Dickinson), followed by FITC anti-mouse (DAKO, Glostrup, Denmark). Cells were then stained with a propidium iodide solution (50µg/ml) containing RNase A (20µg/ml) for 30 min at RT. The samples were processed using FACS Calibur (Becton Dickinson) and the data were analyzed with the Cell Quest software (Becton Dickinson).

DNA fiber assay

DNA replication fork dynamics were investigated on single DNA molecules as Schwab and Niedzwiedz described in 2011.In brief, cells were pulse labeled with 25 µM halogenated nucleotides chlorodeoxyuridine (CIdU), washed and treated with 4.3 mM MMS to induce

replication fork stalling or DMSO as control, then incubated with 250 μM iododeoxyuridine (IdU, Sigma-Aldrich) for 20 min. Harvested cells were diluted to 106 cells/ml. Spreading and staining were performed as described in (51). Fluorescence images were captured using Axioplan 2 fluorescence microscope (Zeiss) and analyzed using the Image J software. At least 50 unidirectional forks labeled with both CldU and IdU were measured for every condition. The elongation ratio was calculated by length of IdU/length of CIdU, quantitatively reflecting the relative changes in replication fork efficiency.

Acknowledgements

This work was supported by the Swedish Cancer Foundation, the Swedish Research Council, the Cancer Society in Stockholm, the Swedish Children Cancer Society, Stockholm County Council and Karolinska Institutet.

The authors thank Mr. Z. Elbeck for assisting with technical work and Dr. Arne Lindqvist for valuable comments on the manuscript.

Conflict of interest

The authors declare no conflict of interest

Authors' contributions

AW, YL and DW performed experiments. AW, YL, EA and OL designed experiments. AW, YL, FH, EA and OL wrote and edited the manuscript. OL is principal investigator.

References

1. Pollak, M. (2012) The insulin and insulin-like growth factor receptor family in neoplasia: an update. *Nature reviews. Cancer* **12**, 159-169
2. Sehat, B., Tofigh, A., Lin, Y., Trocme, E., Liljedahl, U., Lagergren, J., and Larsson, O. (2010) SUMOylation mediates the nuclear translocation and signaling of the IGF-1 receptor. *Science signaling* **3**, ra10
3. Warsito, D., Sjostrom, S., Andersson, S., Larsson, O., and Sehat, B. (2012) Nuclear IGF1R is a transcriptional co-activator of LEF1/TCF. *EMBO reports* **13**, 244-250
4. Warsito, D., Lin, Y., Gnirck, A. C., Sehat, B., and Larsson, O. (2016) Nuclearly translocated insulin-like growth factor 1 receptor phosphorylates histone H3 at

tyrosine 41 and induces SNAI2 expression via Brg1 chromatin remodeling protein. *Oncotarget* **7**, 42288-42302
5. Kelman, Z., and O'Donnell, M. (1995) Structural and functional similarities of prokaryotic and eukaryotic DNA polymerase sliding clamps. *Nucleic acids research* **23**, 3613-3620
6. Carr, A. M., Paek, A. L., and Weinert, T. (2011) DNA replication: failures and inverted fusions. *Seminars in cell & developmental biology* **22**, 866-874
7. Liefshitz, B., Steinlauf, R., Friedl, A., Eckardt-Schupp, F., and Kupiec, M. (1998) Genetic interactions between mutants of the 'error-prone' repair group of Saccharomyces cerevisiae and their effect on recombination and mutagenesis. *Mutation research* **407**, 135-145
8. Motegi, A., Liaw, H. J., Lee, K. Y., Roest, H. P., Maas, A., Wu, X., Moinova, H., Markowitz, S. D., Ding, H., Hoeijmakers, J. H., and Myung, K. (2008) Polyubiquitination of proliferating cell nuclear antigen by HLTF and SHPRH prevents genomic instability from stalled replication forks. *Proceedings of the National Academy of Sciences of the United States of America* **105**, 12411-12416
9. Chang, D. J., and Cimprich, K. A. (2009) DNA damage tolerance: when it's OK to make mistakes. *Nature chemical biology* **5**, 82-90
10. Friedberg, E. C. (2005) Suffering in silence: the tolerance of DNA damage. *Nature reviews. Molecular cell biology* **6**, 943-953
11. Unk, I., Hajdu, I., Blastyak, A., and Haracska, L. (2010) Role of yeast Rad5 and its human orthologs, HLTF and SHPRH in DNA damage tolerance. *DNA repair* **9**, 257-267
12. Andersen, P. L., Xu, F., and Xiao, W. (2008) Eukaryotic DNA damage tolerance and translesion synthesis through covalent modifications of PCNA. *Cell research* **18**, 162-173
13. Hoege, C., Pfander, B., Moldovan, G. L., Pyrowolakis, G., and Jentsch, S. (2002) RAD6-dependent DNA repair is linked to modification of PCNA by ubiquitin and SUMO. *Nature* **419**, 135-141
14. Stelter, P., and Ulrich, H. D. (2003) Control of spontaneous and damage-induced mutagenesis by SUMO and ubiquitin conjugation. *Nature* **425**, 188-191
15. Watanabe, K., Tateishi, S., Kawasuji, M., Tsurimoto, T., Inoue, H., and Yamaizumi, M. (2004) Rad18 guides poleta to replication stalling sites through physical interaction and PCNA monoubiquitination. *The EMBO journal* **23**, 3886-3896
16. Unk, I., Hajdu, I., Fatyol, K., Hurwitz, J., Yoon, J. H., Prakash, L., Prakash, S., and Haracska, L. (2008) Human HLTF functions as a ubiquitin ligase for proliferating cell nuclear antigen polyubiquitination. *Proceedings of the National Academy of Sciences of the United States of America* **105**, 3768-3773
17. Motegi, A., Sood, R., Moinova, H., Markowitz, S. D., Liu, P. P., and Myung, K. (2006) Human SHPRH suppresses genomic instability through proliferating cell nuclear antigen polyubiquitination. *The Journal of cell biology* **175**, 703-708
18. Unk, I., Hajdu, I., Fatyol, K., Szakal, B., Blastyak, A., Bermudez, V., Hurwitz, J., Prakash, L., Prakash, S., and Haracska, L. (2006) Human SHPRH is a ubiquitin ligase for Mms2-Ubc13-dependent polyubiquitylation of proliferating cell nuclear antigen. *Proceedings of the National Academy of Sciences of the United States of America* **103**, 18107-18112
19. Parvaresch, S., Yesilkaya, T., Baer, K., Al-Hasani, H., and Klein, H. W. (2002) 14-3-3 binding to the IGF-1 receptor is mediated by serine autophosphorylation. *FEBS letters* **532**, 357-362

20. Niu, M., Klingler-Hoffmann, M., Brazzatti, J. A., Forbes, B., Akekawatchai, C., Hoffmann, P., and McColl, S. R. (2013) Comparative proteomic analysis implicates eEF2 as a novel target of PI3Kgamma in the MDA-MB-231 metastatic breast cancer cell line. *Proteome science* **11**, 4
21. Pietrzkowski, Z., Sell, C., Lammers, R., Ullrich, A., and Baserga, R. (1992) Roles of insulinlike growth factor 1 (IGF-1) and the IGF-1 receptor in epidermal growth factor-stimulated growth of 3T3 cells. *Molecular and cellular biology* **12**, 3883-3889
22. Pietrzkowski, Z., Lammers, R., Carpenter, G., Soderquist, A. M., Limardo, M., Phillips, P. D., Ullrich, A., and Baserga, R. (1992) Constitutive expression of insulin-like growth factor 1 and insulin-like growth factor 1 receptor abrogates all requirements for exogenous growth factors. *Cell growth & differentiation : the molecular biology journal of the American Association for Cancer Research* **3**, 199-205
23. Wang, S. C., Nakajima, Y., Yu, Y. L., Xia, W., Chen, C. T., Yang, C. C., McIntush, E. W., Li, L. Y., Hawke, D. H., Kobayashi, R., and Hung, M. C. (2006) Tyrosine phosphorylation controls PCNA function through protein stability. *Nature cell biology* **8**, 1359-1368
24. Lin, Y., Liu, H., Waraky, A., Haglund, F., Agarwal, P., Jernberg-Wiklund, H., Warsito, D., and Larsson, O. (2017) SUMO-modified Insulin-Like Growth Factor 1 Receptor (IGF-1R) Increases Cell Cycle Progression and Cell Proliferation. *Journal of cellular physiology*
25. Wang, Y. N., and Hung, M. C. (2012) Nuclear functions and subcellular trafficking mechanisms of the epidermal growth factor receptor family. *Cell & bioscience* **2**, 13
26. Ortega, J., Li, J. Y., Lee, S., Tong, D., Gu, L., and Li, G. M. (2015) Phosphorylation of PCNA by EGFR inhibits mismatch repair and promotes misincorporation during DNA synthesis. *Proceedings of the National Academy of Sciences of the United States of America* **112**, 5667-5672
27. Zhao, H., Chen, M. S., Lo, Y. H., Waltz, S. E., Wang, J., Ho, P. C., Vasiliauskas, J., Plattner, R., Wang, Y. L., and Wang, S. C. (2014) The Ron receptor tyrosine kinase activates c-Abl to promote cell proliferation through tyrosine phosphorylation of PCNA in breast cancer. *Oncogene* **33**, 1429-1437
28. Olsen, H., and Haldosen, L. A. (2006) Peroxisome proliferator-activated receptor gamma regulates expression of signal transducer and activator of transcription 5A. *Experimental cell research* **312**, 1371-1380
29. Das-Bradoo, S., Ricke, R. M., and Bielinsky, A. K. (2006) Interaction between PCNA and diubiquitinated Mcm10 is essential for cell growth in budding yeast. *Molecular and cellular biology* **26**, 4806-4817
30. Prosperi, E., Stivala, L. A., Sala, E., Scovassi, A. I., and Bianchi, L. (1993) Proliferating cell nuclear antigen complex formation induced by ultraviolet irradiation in human quiescent fibroblasts as detected by immunostaining and flow cytometry. *Experimental cell research* **205**, 320-325
31. Zhang, P., Sun, Y., Hsu, H., Zhang, L., Zhang, Y., and Lee, M. Y. (1998) The interdomain connector loop of human PCNA is involved in a direct interaction with human polymerase delta. *The Journal of biological chemistry* **273**, 713-719
32. Maga, G., and Hubscher, U. (2003) Proliferating cell nuclear antigen (PCNA): a dancer with many partners. *Journal of cell science* **116**, 3051-3060
33. Pohlhaus, J. R., and Kreuzer, K. N. (2006) Formation and processing of stalled replication forks--utility of two-dimensional agarose gels. *Methods in enzymology* **409**, 477-493

34. de Feraudy, S., Limoli, C. L., Giedzinski, E., Karentz, D., Marti, T. M., Feeney, L., and Cleaver, J. E. (2007) Pol eta is required for DNA replication during nucleotide deprivation by hydroxyurea. *Oncogene* **26**, 5713-5721
35. Leach, C. A., and Michael, W. M. (2005) Ubiquitin/SUMO modification of PCNA promotes replication fork progression in Xenopus laevis egg extracts. *The Journal of cell biology* **171**, 947-954
36. Yang, X. H., and Zou, L. (2009) Dual functions of DNA replication forks in checkpoint signaling and PCNA ubiquitination. *Cell cycle* **8**, 191-194
37. Valenciano, A., Henriquez-Hernandez, L. A., Moreno, M., Lloret, M., and Lara, P. C. (2012) Role of IGF-1 receptor in radiation response. *Translational oncology* **5**, 1-9
38. Chitnis, M. M., Lodhia, K. A., Aleksic, T., Gao, S., Protheroe, A. S., and Macaulay, V. M. (2014) IGF-1R inhibition enhances radiosensitivity and delays double-strand break repair by both non-homologous end-joining and homologous recombination. *Oncogene* **33**, 5262-5273
39. Baple, E. L., Chambers, H., Cross, H. E., Fawcett, H., Nakazawa, Y., Chioza, B. A., Harlalka, G. V., Mansour, S., Sreekantan-Nair, A., Patton, M. A., Muggenthaler, M., Rich, P., Wagner, K., Coblentz, R., Stein, C. K., Last, J. I., Taylor, A. M., Jackson, A. P., Ogi, T., Lehmann, A. R., Green, C. M., and Crosby, A. H. (2014) Hypomorphic PCNA mutation underlies a human DNA repair disorder. *The Journal of clinical investigation* **124**, 3137-3146
40. Masutani, C., Kusumoto, R., Yamada, A., Dohmae, N., Yokoi, M., Yuasa, M., Araki, M., Iwai, S., Takio, K., and Hanaoka, F. (1999) The XPV (xeroderma pigmentosum variant) gene encodes human DNA polymerase eta. *Nature* **399**, 700-704
41. Stary, A., and Sarasin, A. (2002) The genetics of the hereditary xeroderma pigmentosum syndrome. *Biochimie* **84**, 49-60
42. Stary, A., and Sarasin, A. (2002) Molecular mechanisms of UV-induced mutations as revealed by the study of DNA polymerase eta in human cells. *Research in microbiology* **153**, 441-445
43. Broughton, B. C., Cordonnier, A., Kleijer, W. J., Jaspers, N. G., Fawcett, H., Raams, A., Garritsen, V. H., Stary, A., Avril, M. F., Boudsocq, F., Masutani, C., Hanaoka, F., Fuchs, R. P., Sarasin, A., and Lehmann, A. R. (2002) Molecular analysis of mutations in DNA polymerase eta in xeroderma pigmentosum-variant patients. *Proceedings of the National Academy of Sciences of the United States of America* **99**, 815-820
44. Holzenberger, M., Dupont, J., Ducos, B., Leneuve, P., Geloen, A., Even, P. C., Cervera, P., and Le Bouc, Y. (2003) IGF-1 receptor regulates lifespan and resistance to oxidative stress in mice. *Nature* **421**, 182-187
45. Castells-Roca, L., Mueller, M. M., and Schumacher, B. (2015) Longevity through DNA damage tolerance. *Cell cycle* **14**, 467-468
46. Ermolaeva, M. A., Dakhovnik, A., and Schumacher, B. (2015) Quality control mechanisms in cellular and systemic DNA damage responses. *Ageing research reviews* **23**, 3-11
47. Waraky, A., Aleem, E., and Larsson, O. (2016) Downregulation of IGF-1 receptor occurs after hepatic linage commitment during hepatocyte differentiation from human embryonic stem cells. *Biochemical and biophysical research communications* **478**, 1575-1581
48. Waraky, A., Akopyan, K., Parrow, V., Stromberg, T., Axelson, M., Abrahmsen, L., Lindqvist, A., Larsson, O., and Aleem, E. (2014) Picropodophyllin causes mitotic arrest and catastrophe by depolymerizing microtubules via insulin-like growth factor-1 receptor-independent mechanism. *Oncotarget* **5**, 8379-8392

49. Huang, J., Huen, M. S., Kim, H., Leung, C. C., Glover, J. N., Yu, X., and Chen, J. (2009) RAD18 transmits DNA damage signalling to elicit homologous recombination repair. *Nature cell biology* **11**, 592-603
50. Aleem, E., Kiyokawa, H., and Kaldis, P. (2005) Cdc2-cyclin E complexes regulate the G1/S phase transition. *Nature cell biology* **7**, 831-836
51. Elvers, I., Johansson, F., Groth, P., Erixon, K., and Helleday, T. (2011) UV stalled replication forks restart by re-priming in human fibroblasts. *Nucleic acids research* **39**, 7049-7057

Figure legends:

Figure 1. Insulin-like growth factor receptor (IGF-1R) translocates to cell nucleus and binds to proliferating cell nuclear antigen (PCNA)

(A) WA01 cells (hESC cell line), grown under feeder-free conditions, were harvested and subjected to cell fractionation. The obtained cytoplasm, cell membrane, and nuclear fractions were lysed and analysed for IGF-1Rβ expression using immunoblotting (IB). Membranes were reblotted to determine the purity of the fractions (GAPDH for cytoplasm, calnexin for cell membrane and Histone H2A for nucleus).

(B) Presence of nIGF-1R in hESC nuclei was confirmed using indirect immunofluorescence (2 left panels). hESC cells were incubated with IGF-1R antibody (green), counterstained with DAPI (blue) to visualize nuclei. The negative control was obtained by omitting the primary antibody. Two right panels show the same analysis on R+ (expressing human IGF-1R) and R- (IGF-1R negative) MEF cells. Scale bar, 10μM.

(C) hESC cells were harvested, lysed and immunoprecipitated for IGF-1R β-subunit (IGF-1R) and detected for PCNA (left panel) or immunoprecipitated for PCNA and detected for IGF-1Rβ (right panel). IgG was used as negative control.

(D) hESC cells were analysed for subcellular localization of IGF-1R–PCNA complexes by in situ PLA (see Materials and methods for details). hESC Red dots indicate IGF-1R–PCNA

interactions. Counterstaining with DAPI (blue) visualizes cell nuclei. The negative control was obtained by omitting one of the primary antibodies. Scale bar, 5μM.
(E) R+ and R- cells were immunoprecipitated for PCNA and detected for IGF-1R and PCNA by immunoblotting. See also Figure S2B showing this Co-IP in comparison to expression of IGF-1R and PCNA in the whole cell lysates.
Data are representative of three or more independent experiments.

Figure 2. IGF-1R phosphorylates PCNA

(A) R+ and R- cells, grown under basal conditions until subconfluency,were harvested, lysed and immunoprecipitated for PCNA and detected for phospho-tyrosine (P-Tyr) (top panel). Blot was stripped and incubated with anti-PCNA. Cells were also immunoprecipitated for P-Tyr and detected for PCNA (bottom panel).
(B) His-Tag recombinant PCNA was subjected to an in-vitro phosphorylation reaction using recombinant IGF-1R kinase in presence or absence of ATP. The reactions were terminated by boiling in SDS sample buffer. Separation of samples in 4-12% SDS–PAGE, followed by IB with a P-Tyr antibody. Reblotting was made for detection of IGF-1R kinase and His-Tag PCNA. As indicated, negative controls were obtained by omitting recombinant IGF-1R kinase, recombinant His-Tagged PCNA or ATP from the reactions. Data are representative of three or more independent experiments.
(C) Diagrammatic representation of peptide coverage and PTMs in PCNA with (lower panel) or without (upper panel) IGF-1R kinase domain as observed by LC-MS/MS. Peptides and phosphorylation sites with high coverage are presented in green, those with low coverage are presented in yellow or pink. Y60, Y133 and Y240 are highlighted by arrows.
(D) R+ cells were treated with 1μM NVP-AEW541 (NVP), 100ng/ml IGF-1, or vehicle for 3h and 24h, in comparison with non-treated R- cells. Cell lysates were separated on 4-12% Bis-Tris SDS-PAGE and subjected to immunoblotting with a PCNA antibody. Tubulin was used as loading control.

Figure 3. IGF-1R phosphorylation is essential for ubiquitination of PCNA

(A) R+ and R- cells were harvested, lysed and immunoprecipitated for PCNA and detected for ubiquitin. Blots were stripped and incubated with anti-PCNA to confirm equal loading.

(B) R+ cells were treated with either1μM NVP, 100ng/ml IGF-1 or vehicle for 3h, in comparison with non-treated R- cells. PCNA was immunoprecipitated from cells and blotted for Ub. Reblotting for P-Tyr and PCNA.
(C) R+ and R- cells were immunoprecipitated for PCNA and detected for SHPRH, HLTF, UBC13, RAD18 or Pol η. Blots were stripped and incubated with anti-PCNA. (R-) was used as negative control. See Figure S6A for expression of ligases in the whole cell lysates.
(D) Immunoprecipitation of green-fluorescent protein (GFP) in R+ cells transfected with wild type (WT) or mutated tyrosine residues (Y1-3) *PCNA-GFP*. Y1 = Y60F, Y2 = Y133F, Y3 = Y250F and Y1-2-3 = triple mutant (Y60F+Y133F+Y250F). Mock transfected R+ cells were used as a negative control. Membranes were immunoblotted for IGF-1R, Ub, P-Tyr, SHPRH, HLTF, RAD18 and PCNA. See Figure S6B for expression of ligases in the whole cell lysates. Data are representative of three or more independent experiments.

Figure 4. IGF-1R regulates ubiquitination of PCNA and replication fork progression after induced DNA damage

(A) R+ and R- cells, grown under basal conditions, were treated with 1μM NVP or vehicle for 1h, followed by UV irradiation with *30 mJ*/cm2 for 30 seconds and 1h non-treatment incubation. Non-irradiated cells represent negative controls (Ctr). PCNA was immunoprecipitated from the cell lysates and subjected to IB for detection of Ub. Blots were stripped and incubated with anti-PCNA to confirm equal loading.
(B) Left panel depicts a schematic diagram of protocol used for DNA fiber assay. Cells were pulse-labeled with halogenated nucleotides CldU (red) and IdU (green) for 20 min each. Using MMS, which interferes with DNA replication during the second pulse-labeling (IdU), fork elongation/stalling in response to replicative stress is detected. Right panel shows stained appearance of fork events as detected by DNA fiber assay.
(C) DNA fibers labeled with CIdU (red) and IdU (green), as described in schematic diagram, used to measure replication fork restart after treating (R+) and (R-) cells with vehicle or 4.3mM MMS for 20min (left-panel). For details see Materials and methods. Right panel shows graphical presentation of replication restart speed as the ratio of the lengths of nascent replication tracts after inducing DNA damage labeled with IdU (green) to the length of the replication tract before inducing damage labeled with CIdU (red). At least 50 unidirectional forks labeled with both CldU and IdU were measured for each condition. Scale bar, 5 μM. Data represent mean ± SD of three independent experiments and considered significant (*) at $P < 0.01$, using one-way ANOVA.

Figure 5. IGF-1R is required for cell cycle progression after induced DNA damage

(A) FACS analysis of (R+) and (R-) cell lines, labelled with BrdU and stained with PI after 6 h treatment with either 1.2mM MMS or DMSO. Cells were synchronized at G1 by serum starvation for 24h, and then released in full medium for 12h for maximal S-phase synchronization before treatment.

(B) Graphic presentation of cell cycle distributions of DMSO- and MMS-treated cells. Data represent mean ± SD of three independent experiments and considered significant (*) at $P < 0.01$, using two-sided t-test. NS, not significant.

(C) Unsynchronized R+ and R- cells were pulse labeled with BrdU for 1h, followed by washing the cells from BrdU labelling and the subsequent treatment with either MMS or DMSO for 6h. Cells were fixed, stained for BrdU and DAPI and processed to flow cytometry. The BrdU labeled cells were gated (green dots) from non-BrdU labeled cells (red dots).

Figure 6. IGF-1R-PCNA interaction and associated PCNA modifications in various cell lines

(A)IGF-1R-PCNA interaction in indicated cell lines (SNL, Gm02808 and hESC) was determined by co-immunoprecipitation. Membranes were reblotted for IGF-1R for equal loading. R+ and R- were used as positive and negative controls, respectively.

(B-C) Immunoprecipitates of PCNA from SNL, Gm02808 and hESC cells were immunoblotted for P-Tyr, Ub and PCNA (B) and E2/E3 ligases (C). R+ and R- cells were used as controls.

(D) Western blot analysis showing expression of the indicated ligases (cf. Figure 6C) in whole cell lysates.

Data are representative of three or more independent experiments.

Figure 7. Schematic model of suggested IGF-1R/PCNA regulation of DDT pathway.

(A) Side and front views of the crystal structure of unmodified proliferating nuclear antigen (PCNA) from *Homo sapiens*. The PCNA monomers are shaded in lime, grey and cyan. The tyrosine Y^{60} is shown in violet, the Y^{133} in blue and the Y^{250} in green. The interdomain connecting loop (IDCL) is shown in orange.

(B) IGF-1R/PCNA regulation of DDT. See text.

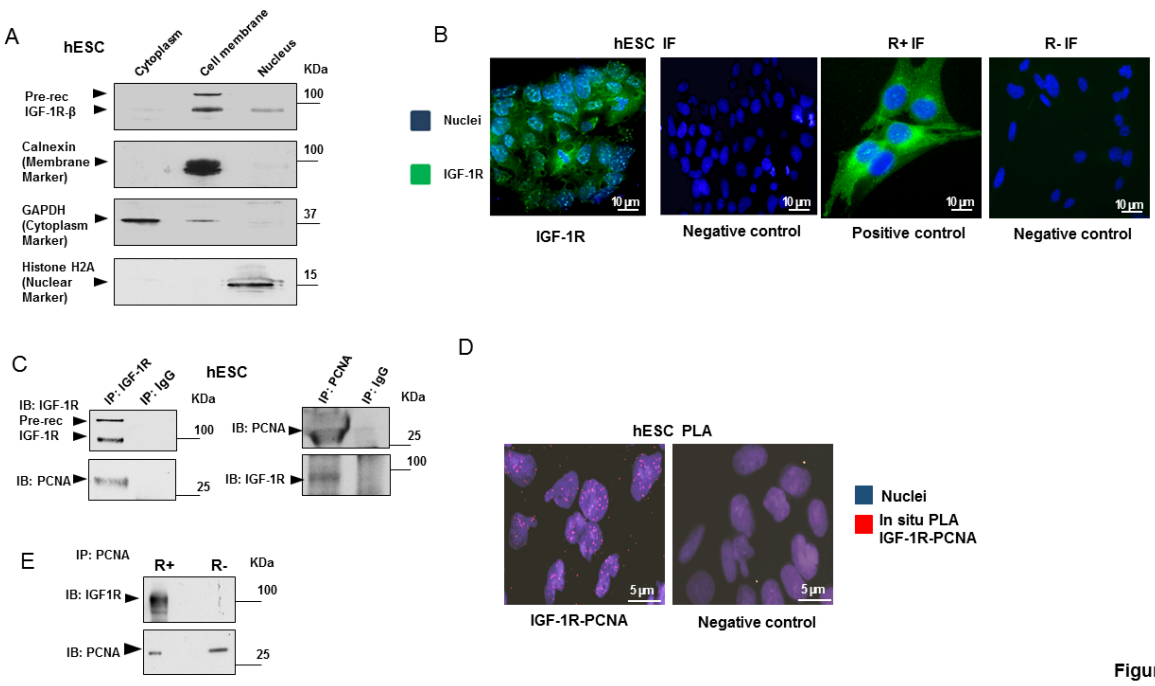

Figure 1

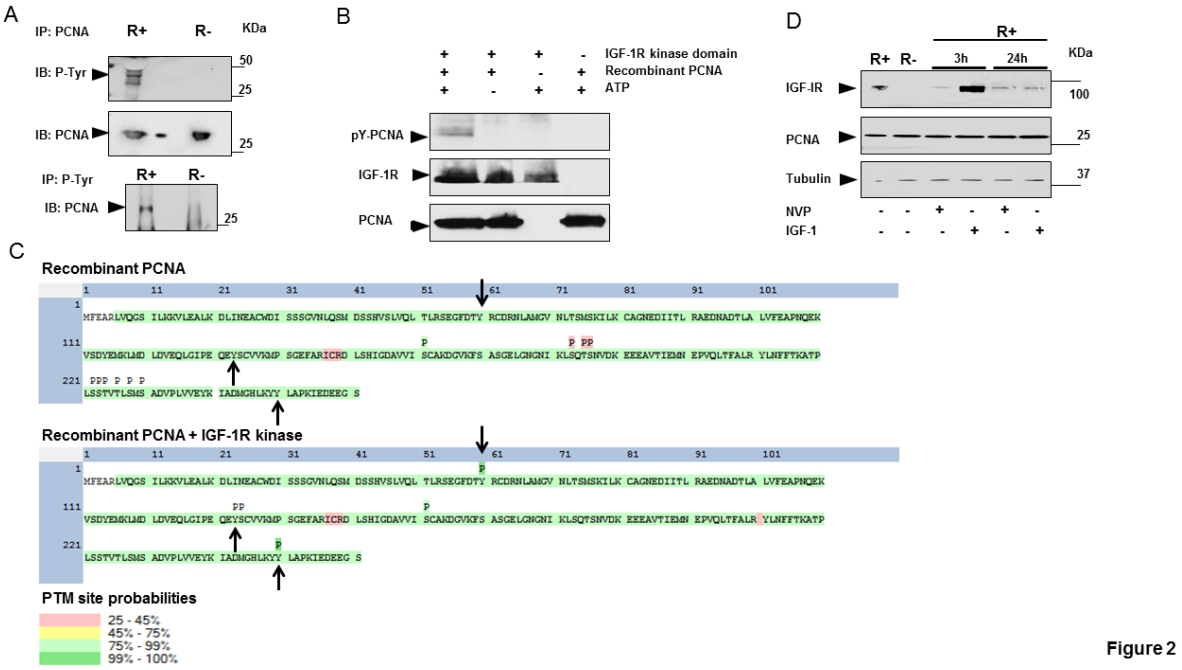

Figure 2

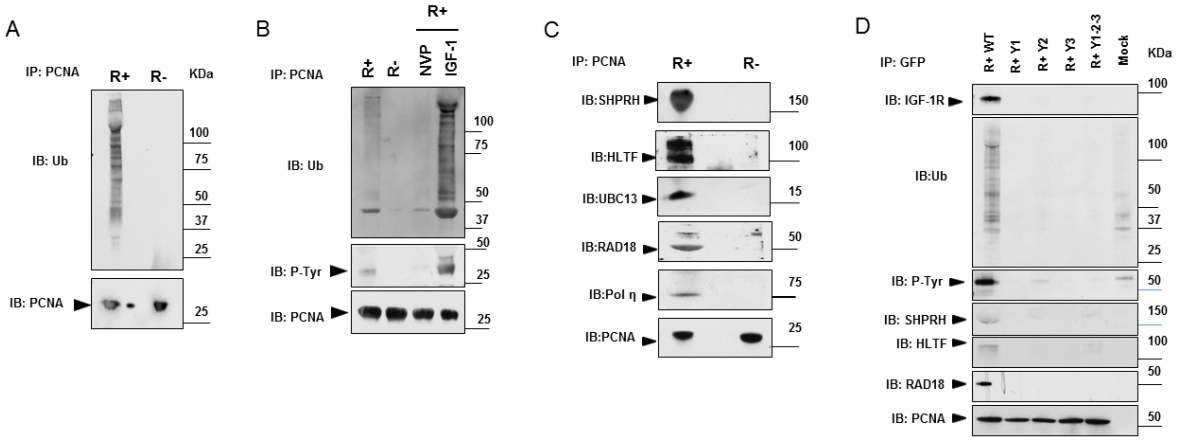

Figure 3

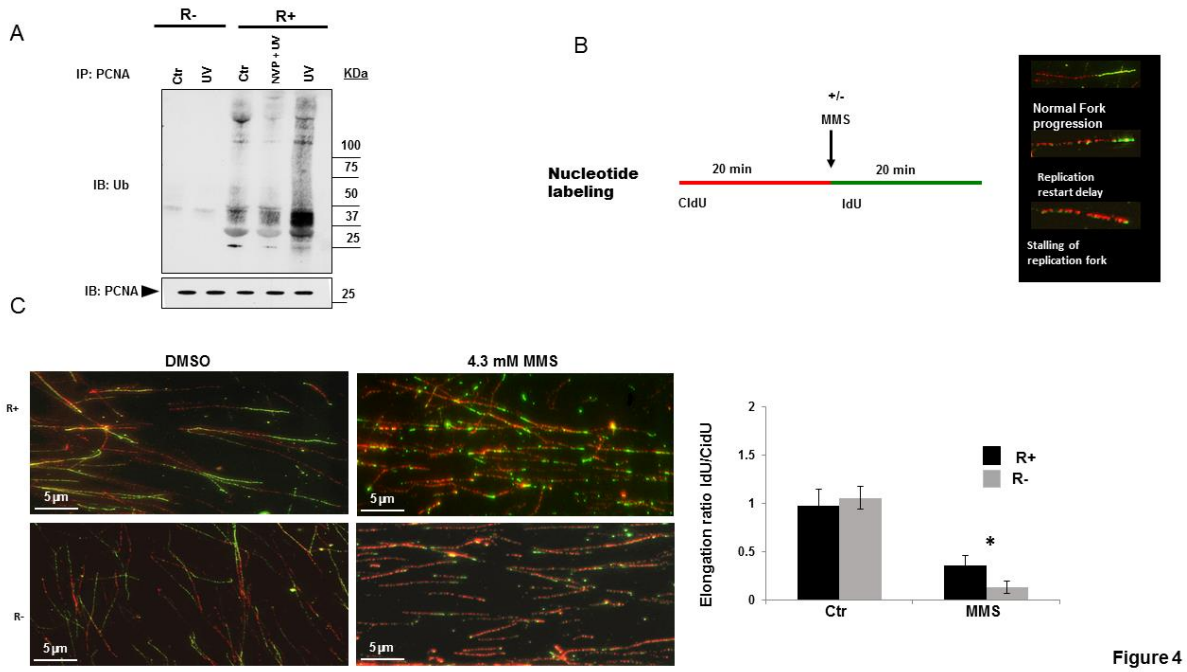

Figure 4

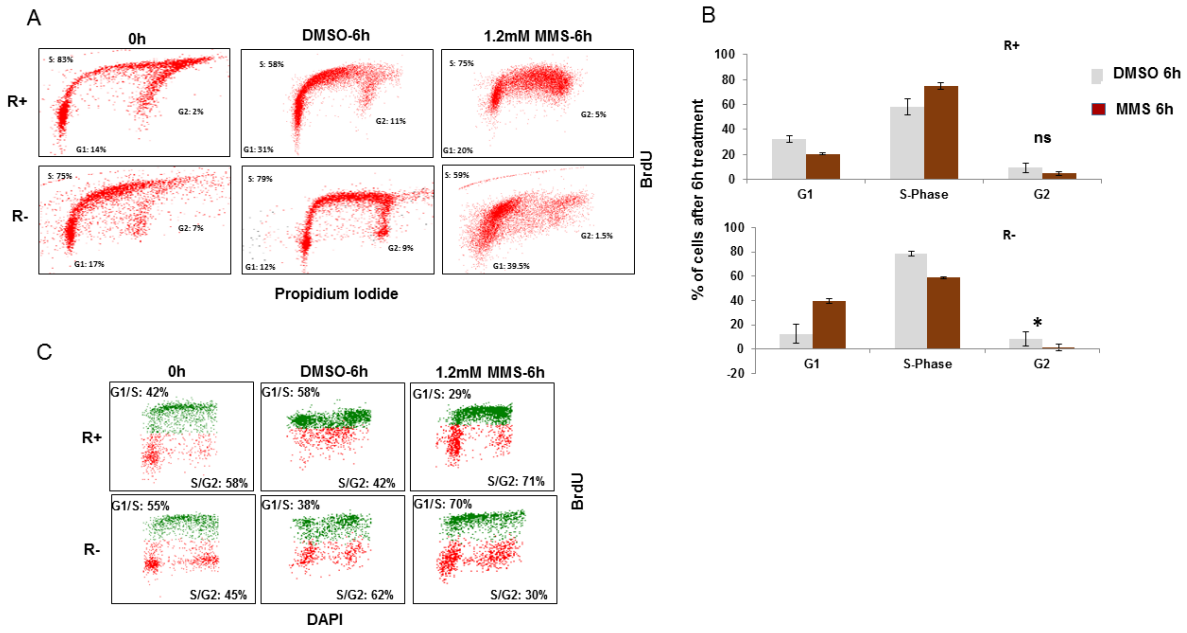

Figure 5

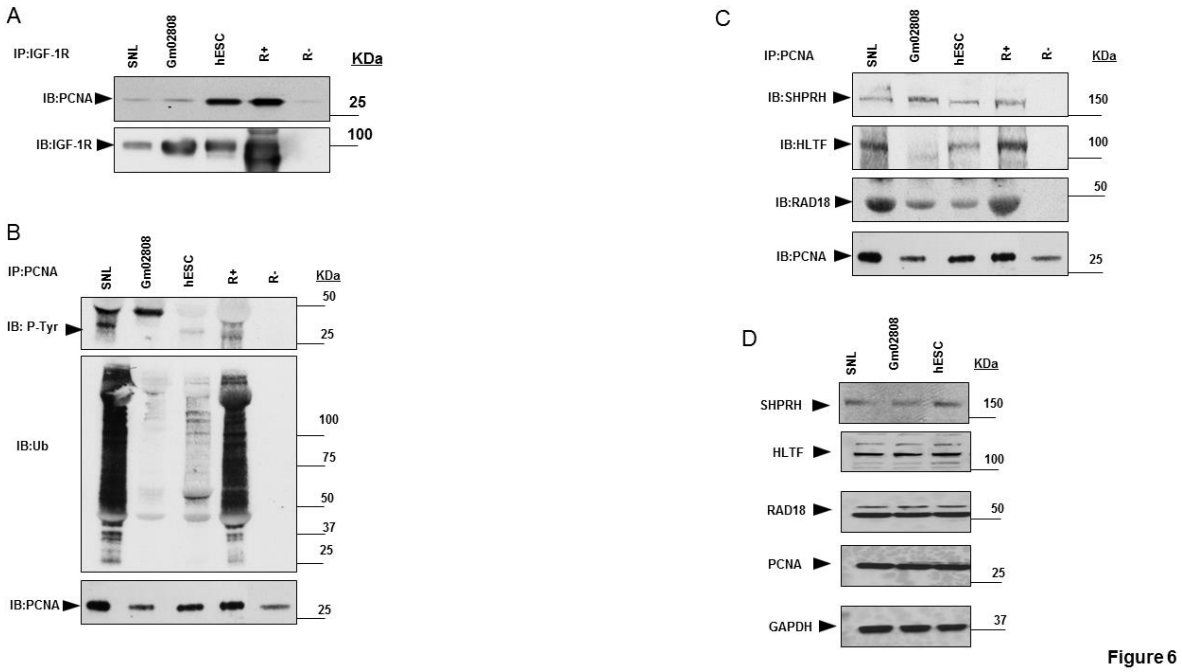

Figure 6

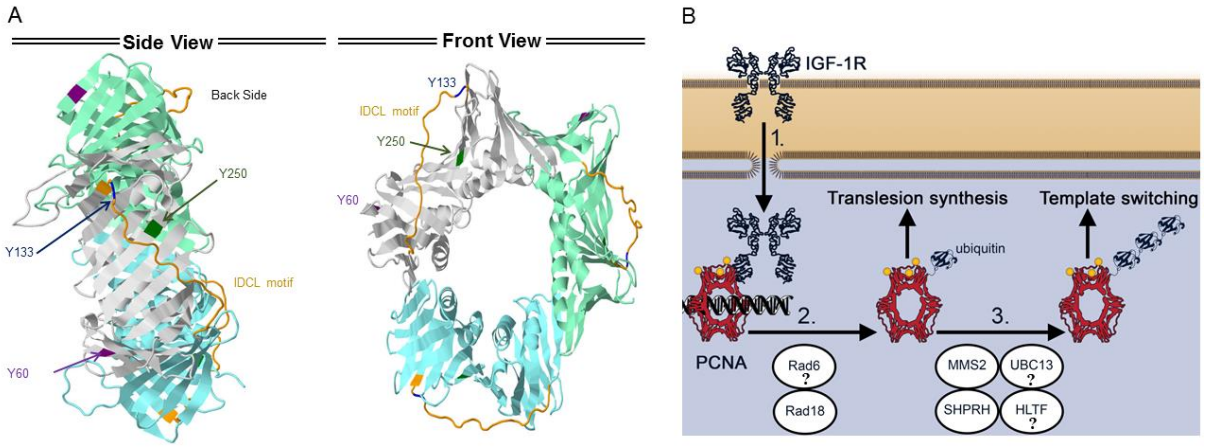

Figure 7

Nuclear insulin-like growth factor 1 receptor phosphorylates proliferating cell nuclear antigen and rescues stalled replication forks after DNA damage

Ahmed Waraky, Yingbo Lin, Dudi Warsito, Felix Haglund, Eiman Aleem and Olle Larsson Sr.

J. Biol. Chem. published online September 18, 2017
